International Journal of Remote Sensing
Vol. 27, No. 7, 10 April 2006, 1367–1393

A neural network integrated approach for rice crop monitoring

C. CHEN*† and H. MCNAIRN‡
†Devel-Tech Inc, 100–2103 Airport Drive, Saskatoon, Saskatchewan, Canada S7L 6W2
‡Agriculture and Agri-food Canada, 960 Carling Ave., Ottawa, Canada K1A 0C6

(*Received 17 August 2004; in final form 23 March 2005*)

Within Asia, rice is a main source of nutrition and provides between 30 and 70% of the daily calories for half the world's population. The importance of rice production demands an effective rice crop monitoring system to provide food security for this region. Recent research has proven radar's capabilities in rice crop monitoring. Radar backscatter increases significantly during a short period of vegetation growth, but large spatial variations in rice crop growth occur due to shifting in the crop calendar. The significant increase in radar backscatter over a short period of time can be used to differentiate rice fields from other land covers. The inter-field variations can be used to derive information on local farmer practices and to enhance rice field mapping and yield prediction. The rice crop monitoring system developed in this project was based on these variations as applied to a neural network classification. The system delineated rice production areas for one wet and one dry season, and was able to extract information on rice cultivation as a function of different planting dates. A minimum mapping accuracy of 96% was achieved for both seasons. This information was then used in a neural network-based yield model to predict rice yield on a regional basis for the wet season. When the yields predicted by the neural network were compared with government statistics, the result was a prediction accuracy of 94%.

1. Introduction

Rice forms the economic, cultural, and nutritional basis for many countries, making this crop's successful annual production of key significance to the world community. Recent projections made by the International Rice Research Institute (1998) show that demand for rice will increase by about 1.8% per year until 2025. This means that over the next two decades, rice consumption will increase by approximately 40%. Most of this increased demand is occurring in Asian countries in response to a population growth that is also expected to increase by as much as 44% over the same time period, based on a 1.6% growth rate between 1980 and 1998 (The World Bank Group 2000). Given that a rising population reduces the land available for production, the only means of meeting this demand is by increasing yield per hectare through improved varieties and cropping practices. Improvements in this area have already resulted in potential yield increases from 3.5 metric tonnes (MT)/hectare to as high as 10–11 MT/hectare in some regions (International Rice Research Institute 1998). Also, the introduction of new varieties has substantially reduced the length of the rice growing cycle. Despite yield improvements, it seems likely that many South-East Asian countries, such as Malaysia, the Philippines, and Vietnam, will not be

*Corresponding author.

International Journal of Remote Sensing
ISSN 0143-1161 print/ISSN 1366-5901 online © 2006 Taylor & Francis
http://www.tandf.co.uk/journals
DOI: 10.1080/01431160500421507

able to grow enough rice to meet domestic needs. This situation raises severe questions regarding food and economic security for these countries. An example of these implications occurred in the Philippines when in 1995 an unexpectedly severe rice shortage resulted in spiralling rice prices, such that local market prices rose 50% above world prices (International Rice Research Institute 1997). Estimating shortfalls and importing the difference to control domestic prices is now an important policy for the government in the Philippines. This policy requires accurate and immediate knowledge of potential rice production throughout the growth cycle, along with an aggressive approach to increasing yield. Given the potential savings in monetary, environmental, and human terms that could be realized by access to accurate prediction of rice yields, the market for a rice growth monitoring service is substantial.

The major stumbling block in the development of an accurate rice monitoring programme is to gather data required for forecasting. Use of remotely sensed data has proven to be a very effective method of gathering this type of information for a wide variety of crops around the world. Most of this work, however, has been done using optical satellite data, which can be rendered ineffective under poor weather conditions. Most rice production in South-East Asia occurs under monsoon conditions and even the 'dry season' skies are often covered with haze and high-level cloud. Synthetic Aperture Radar (SAR) images, on the other hand, are not hindered by most weather conditions and will be able to provide imagery over the entire crop growth cycle. Scientific evidence has demonstrated two key points in regards to the potential use of SAR as part of a rice monitoring system. This research has demonstrated a high correlation between radar backscatter and rice biomass, and has established that fields under rice production can be accurately mapped based on temporal variation in radar backscatter (Aschbacher *et al.* 1995, Brisco and Brown 1995, Kurosu *et al.* 1995, Le Toan *et al.* 1997, Ribbes and Le Toan 1999, Inoue *et al.* 2002). Rice fields exhibit a unique temporal backscatter signature over the growth cycle of the crop. The increase in backscatter as the rice crop matures is primarily due to the vegetation–water interaction. Backscatter increases approximately 8 dB from the beginning of its growing cycle until maturity (Liew *et al.* 1998). With this unique signature, SAR backscatter can be related to crop biomass and can be used to map fields under rice production. Li *et al.* (2003) successfully mapped land cover with a simple supervised classification of a RADARSAT-1 ScanSAR image acquired over South China. The average accuracy for identifying rice fields was 90%.

Like most other crops, planting date varies among rice fields. The rice calendar is significantly affected by temperature differences due to latitude (Li *et al.* 2003). The resulting differences in planting dates create inter-field differences in crop growth and, as a result, large variations in radar backscatter. These variations complicate the use of SAR imagery for mapping rice fields. Le Toan *et al.* (1997) found that the standard classification methods based on the similarity in the image intensity of rice fields did not provide acceptable results. They proposed and tested a temporal change measurement method to cope with inter-field variations. Liew *et al.* (1998) used a similar approach to delineate and map areas under different rice cropping systems in the Mekong River Delta, Vietnam. In their research, they created five change index maps from seven ERS-2 images acquired during a rice production season. By combining these five change index maps and using a 3 dB threshold, a total of 243 possible classes could be formed. The final rice cropping systems were created by merging the dominant change classes and discarding the minority classes. Ribbes and Le Toan (1999) later applied a similar approach to RADARSAT-1 data.

Based on the temporal change of the backscatter, rice fields were mapped to an 87% level of accuracy.

Neural networks as a tool in the field of remote sensing have received considerable attention since a new learning scheme was developed. The principle of a back propagation of error learning algorithm was initially proposed by Werbos (1974) and rediscovered independently by Parker (1985) and Rumelhart *et al.* (1986). Since the early nineties, numerous researchers have compared the performance of neural networks with conventional statistical approaches to remote sensing applications. Benediktsson *et al.* (1990) evaluated the two methods for multisource remote sensing data classification. They noted that a neural network has great potential as a pattern recognition method for multisource remotely sensed data because of the distribution-free nature of a neural network. In addition, no prior knowledge is needed about the statistical distributions of the classes in the data sources. Bischof *et al.* (1992), as well as Paola and Schowengerdt (1995), compared methods for multispectral classification of Landsat TM data and both found that, with proper training, a neural network was able to perform better than the maximum likelihood classification. Foody *et al.* (1995) and Chen (1996) used a neural network to classify agricultural crops from synthetic aperture radar data and found that, in general, neural network classifications were equal to or more accurate than those derived from the discriminant analysis. Shao *et al.* (2001) used multitemporal RADARSAT-1 data and a neural network classifier to map land cover in China. The accuracy of the rice classification was 91%, 97% after post-classification filtering. Chen (1997) tested different neural network structures and network parameters to monitor wheat crop growth based upon RADARSAT-1 images and found that a two-layered neural network (where the number of neurons in the first hidden layer is equal to, or greater than, the input features and where the number of neurons in the second hidden layer is neither close to that of the first hidden layer nor close to that of the output layer) can provide better biomass detection on both training and testing data. The experiment showed that the accuracy on training data increases as learning iterations, learning rate, and momentum increase, whereas the accuracy on testing data is more sensitive to the learning iterations than the changing of learning rate and momentum.

In practical applications such as rice monitoring over an extended region, it is usually impossible to acquire detailed ground data to cover all the variations, such as rice cultivation time, variety, and management aspects. Over two years, in partnership with the Philippine Rice Research Institute (PhilRice), an approach for rice mapping was developed that combines change detection with neural networks. This approach offers flexibility with respect to the requirement for ancillary data and can be applied to a more extended area. Such an approach provides an operational potential for rice field mapping. This paper describes the radar backscatter patterns as a function of planting date and rice growth development, for one wet and one dry growing season. For each of these growing seasons, the performances of three approaches for rice mapping were tested for two sites in the Philippines. These three approaches included a neural network, change detection, and maximum likelihood classification. Based on these results, a new approach to rice mapping is proposed comprising an integration of the change detection and neural network methods. Finally, this paper investigates the prediction of rice yield using a neural network.

2. Data collection and processing

2.1 *Study site*

Two sites in the Philippines were used to develop and test the methodologies, one in the vicinity of the city of Muñoz and the second near the city of Santo Domingo. Both cities are located in the northern part of the province of Nueva Ecija, approximately 147 kilometres north of Manila in the Philippines (figure 1). Santo Domingo is south-west of Muñoz where PhilRice is located. The lands around both Muñoz and Santo Domingo are mostly agricultural. The percentage of land devoted to rice production in the two regions is approximately 45% and 66%, respectively. Two rice production seasons per year are the common practice. The typical size of a rice field is about 0.7 to 1.25 hectares. The terrain of these two regions is generally flat, with slopes of between 0–3%. The soils are classified as La Paz Fine Sandy-Loam, Antipolo Clay, and Quingua Silt-Loam.

The seasons in Nueva Ecija are denoted as dry (January–April) and wet (June–September), with monthly rainfall around 30 mm and 370 mm, respectively. During the dry season, rainfall is minimal and there are very few typhoons. Annual temperatures range from 20°C to 35°C. Many farmers directly seed (hand broadcast) their rice during the dry season as there is less risk of damage and the cost is less compared to transplanting seedlings. The wet season is characterized by frequent rain showers and typhoons. The fields are flooded for most of the season. The heavy rain and strong winds cause substantial loss of seedlings and wash away insecticides and fertilizers. Farmers try to minimize the impact of the typhoons by transplanting rice seedlings rather than using direct seeding. Farmers that seed directly usually experience lower yields at harvest.

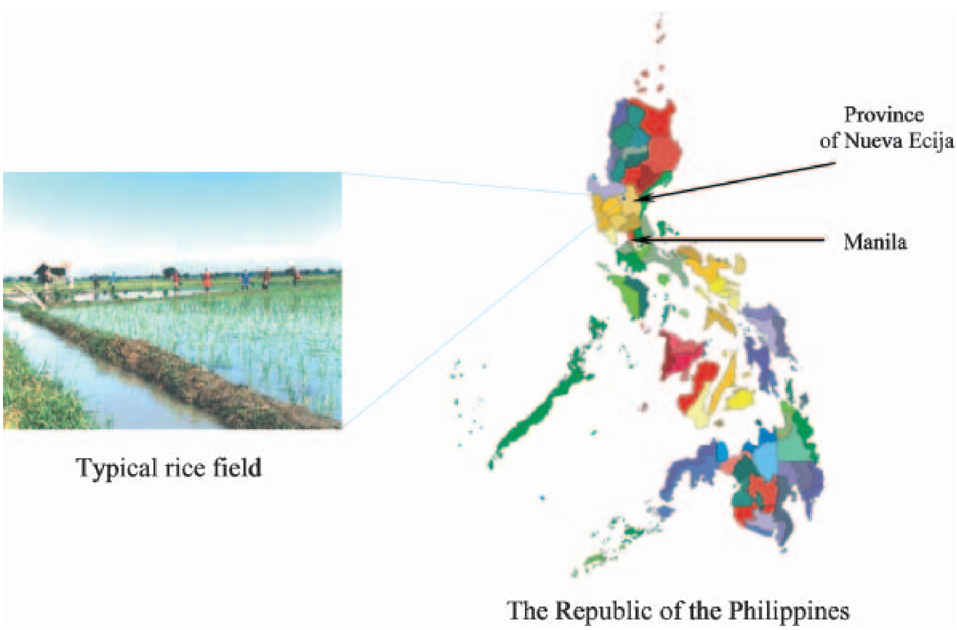

Figure 1. Location of the study site within The Republic of the Philippines.

2.2 *Field data collection*

The project covered two rice-growing seasons in 2001. The dry season covered January to May 2001, and the wet season June to September 2001. A total of 56 rice plots (fields) were used in each season. These plots were managed according to three control schemes (*A*, *B* and *C*). Eighteen *A* plots were strictly managed with three different rice varieties grown under optimal management strategies. Management strategies were optimized for plot geometry, rice variety, time of planting, and water management and these strategies were predefined by PhilRice prior to each crop season. Each rice variety was replicated over six plots. Eighteen *B* plots consisted of experimental, demonstration, and seed production plots that were utilized by the researchers in PhilRice. Twenty *C* plots were selected from farmers' fields in the regions and the management of these plots was not controlled for the purposes of this experiment. The impact on variations of crop calendar was assessed by staggering the transplanting dates of Control *A* plots and by recording the transplanting/seeding dates of all the other experimental plots. All the experimental plots, except one *B* and four *C* plots, which were directly seeded, were transplanted during the wet season. In the dry season, about one half of the plots were transplanted, which included all the *A* plots, eight *B* plots, and two *C* plots.

Both field and sample data were collected from each plot. The field data were collected periodically during each season and these data described general physical characteristics, the management applied, the crop variety, and crop growth stages. The sample data characterized changes in the crop during the growing season. The collected sample data included plant density (plant stems/m^2), plant height (cm), plat dry and wet biomass (g), Leaf Area Index (LAI), water depth (cm) and temperature (°C), and yield (kg/m^2 and kg/ha). A destructive method was used to measure the crop biomass and LAI. To establish wet and dry biomass, the plants were cut around the root zone (at the water surface) in a 1 m^2 area and weighed before and after oven-drying for 24–48 hours at 100°C. The LAI was obtained by passing sample leaves through a leaf area metre and then dividing the total leaf area by ground area. Both grain yield and grain-to-straw ratio were measured by harvesting crops from a 1 m^2 area. The harvested samples were weighed and then threshed. After threshing, the grains were weighed again to calculate the grain-to-straw ratio. The threshed grains were sun dried for 5–8 hours. According to PhilRice's standard, unit grain yield (kg/m^2) and grain yield per hectare (kg/ha) were recorded at 14% moisture content. To characterize the crop condition for the entire plot, four samples were collected from each plot and the average of the measurements from these four samples was used to represent the rice growth of the entire field. Samples were collected coincident with each SAR acquisition.

The boundaries of each plot and sampling location were recorded using a GeoExplorer GPS unit. Daily weather data were also collected from three weather stations near the experimental plots in Nueva Ecija.

2.3 *Image acquisition and pre-processing*

Since the rice fields are usually quite small, often less than one hectare, RADARSAT-1 fine mode images were chosen for this project. The nominal resolution of the fine mode RADARSAT-1 data was $8\,\mathrm{m} \times 9\,\mathrm{m}$ (azimuth $\times$ range). Before each season started, a detailed RADARSAT-1 image acquisition schedule was planned under the following considerations:

1. the schedule should be designed according to the staggered planting intervals associated with Control *A* plots;
2. for each staggered interval, the first image should be acquired one or two days before crop transplanting occurs;
3. the schedule should be consistent with the local farmers' practices and should address their cropping calendar; and
4. if possible, the images should have the same orbital specifications, with the same incident angle and viewing direction, and the images should cover the entire study area without requiring mosaicking.

In order to maintain the same orbital specifications, images must be acquired at a 24-day interval. Based on knowledge of the growth cycle, it was decided that this image acquisition interval was too coarse to capture the rapid changes in the rice growth, particularly early in the season. Thus, a shorter acquisition interval was chosen (table 1).

This shorter interval meant that incident angles and look directions varied among the images acquired; however, this mixture of images likely reflects the reality under operational mapping conditions. The difference in incident angle between the two fine mode products was approximately four degrees. Due to a RADARSAT-1 payload anomaly, the image on 11th February, 2001 was unrecoverable. Thus, the backscatter for 11th February was interpolated using a 2nd order polynomial function and all the available data. Two IRS 1C panchromatic scenes were also acquired to facilitate the geo-referencing of all RADARSAT-1 images.

Image pre-processing included image geo-referencing, radar speckle reduction, and radar backscatter extraction. Although the study region was relatively flat, all the images were ortho-rectified with ground control points selected from 71 GPS points and a digital elevation model (DEM). The DEM was created from scanned 1:50,000 topographic maps. With the help of the DEM, an average 1–1.5 pixel RMS accuracy was achieved. A 5×5 gamma filter was used to reduce radar speckle, and average radar backscatter was extracted for each plot from all the ortho-rectified images.

3. Temporal radar backscatter characteristics of rice

During its growth cycle, a rice plant completes three distinct phases, namely vegetative, reproductive, and ripening. The vegetative phase is subdivided into

Table 1. RADARSAT-1 image acquisition schedules for the 2001 rice crop seasons.

Dry Season			**Wet Season**		
Date of acquisition	Mode	Orbit	Date of acquisition	Mode	Orbit
2001–01-Jan	F1	Asc	2001–11-Jun	F3	Asc
2001–06-Jan	F1	Desc	2001–23-Jun	F1	Desc
2001–18-Jan	F3	Asc	2001–05-Jul	F3	Asc
2001–30-Jan	F1	Desc	2001–17-Jul	F1	Desc
2001–11-Feb	F3 (unusable)	Asc	2001–29-Jul	F3	Asc
2001–23-Feb	F1	Desc	2001–10-Aug	F1	Desc
2001–07-Mar	F3	Asc	2001–22-Aug	F3	Asc
2001–31-Mar	F3	Asc	2001–03-Sep	F1	Desc
2001–24-Apr	F3	Asc	2001–15-Sep	F3	Asc
2001–18-May	F3	Asc	2001–09-Oct	F3	Asc

germination, early seedling growth, and tillering; the reproductive phase is subdivided into the time before and after heading. The time after heading is better known as the ripening period, which consists of the milky and maturity phases. Rice growth is thus characterized by eight stages: tillering, end of tillering, panicle initiation, booting, flowering, milking, maturity, and harvest. The three varieties of rice grown in the experimental plots were Rc82 (early mature variety), IR64 (medium mature variety), and Rc18 (late mature variety). The growth period or lifespan of these rice varieties is 110, 113, and 123 days, respectively.

Figure 2 provides the radar backscatter response to rice growth as a function of rice variety (Rc82, IR64, Rc18) and rice cultivation date (early, middle, and late transplanted). The three charts on the left illustrate the backscatter behaviour during the dry season, and those on the right show the backscatter response during the wet season. The bottom schematics provide an approximation of the rice growth stages for the dry and wet seasons. The horizontal axis for all plots marks the days after transplanting, demonstrating the relationship between radar backscatter and the crop growth stages. In general, the response of the rice crops transplanted in the dry season was more sensitive to a transplanting delay of 12 days (from early to late January). For the rice transplanted in early January, lower backscatter was observed for the ascending passes (F3) acquired at a shallower incident angle. The difference in backscatter between the F1 (descending) and F3 (ascending) passes was less pronounced at more advanced growth stages and for rice fields transplanted later in the season. A smaller difference in backscatter was observed in the wet season when late transplanted and early transplanted crops were compared. The crops took 3–4 days longer to complete each phase of vegetation, reproduction, and ripening in the wet season compared to the dry season. Variations in backscatter as a function of crop variety (Rc82, IR64, Rc18) were small.

Radar backscatter changed as the rice crop moved from one growth stage to the next. Prior to transplanting, with a backscatter of approximately -16 dB, the recorded radar signal was very low due to specular reflection from the flooded fields. At this stage, rice fields were easily detected on the radar images because of the significant backscatter difference between flooded areas and non-flooded areas. During the vegetation phase, the radar backscatter increased. Volume scattering from within the rice canopy, and multiple reflections between the plants and water surface, resulted in an increase in backscatter from around -16 dB to approximately -8 dB in a 22–24 day period (figure 2). This is traditionally the stage for growth monitoring. As the crop ripened, the plant water content decreased. A reduction in backscatter correlated with a reduction in plant water content, with backscatter decreasing from -8 dB to -10 dB. The backscatter reached a minimum prior to harvest. This temporal backscatter pattern is unique to rice crops. Variations in backscatter over the growing season for rice are much larger relative to any other agricultural crop (Aschbacher *et al.* 1995). Retrieval of rice acreage exploits this unique backscatter signature.

4. Estimating rice acreage

One objective of this project was to develop a rice mapping system to estimate, on a regional basis, the acreage under rice production. Mapping rice fields is also a fundamental step for growth monitoring and yield prediction. A key consideration for rice mapping is the spatial variation in the timing of the crop vegetation phase. This vegetation phase usually lasts 20–24 days (figure 2). Due to factors that include

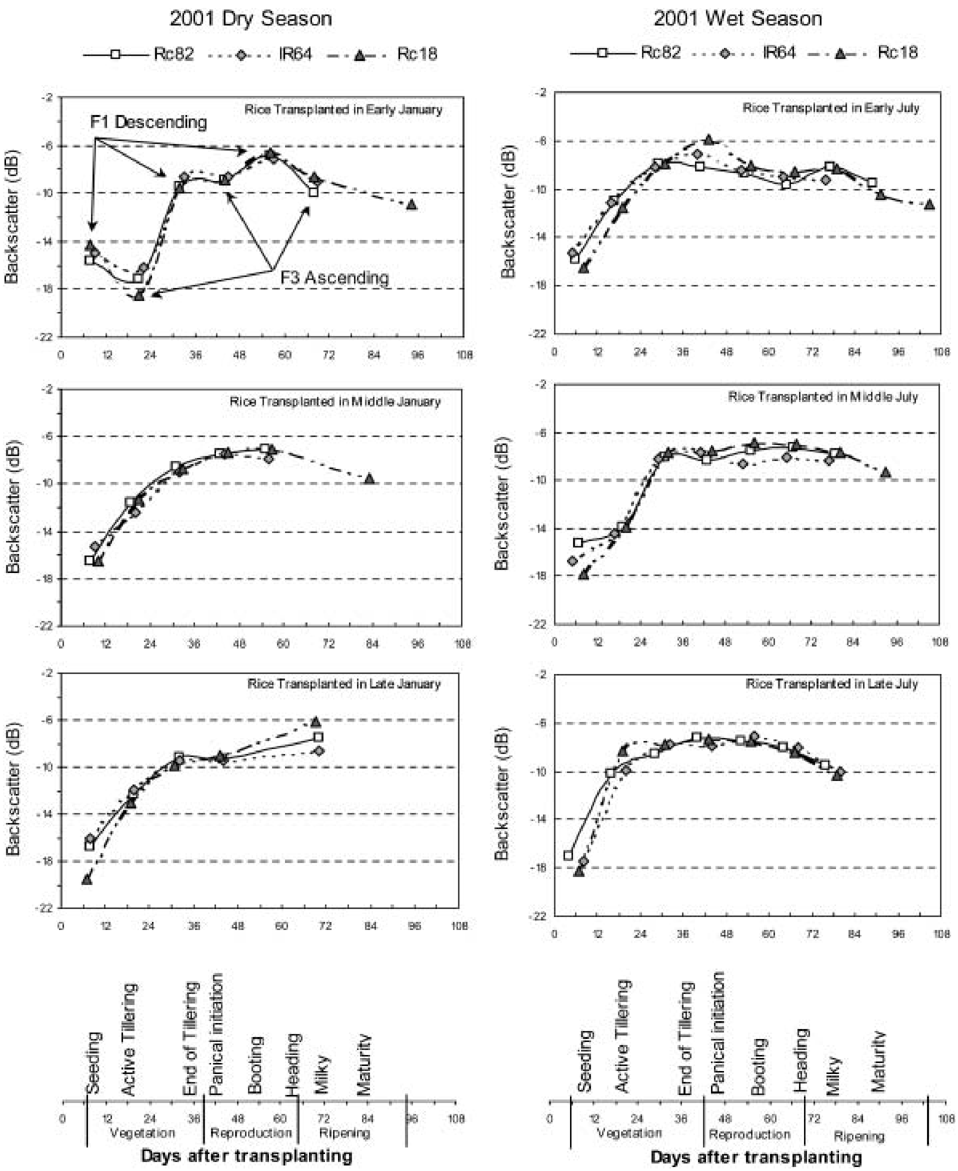

Figure 2. Radar backscatter as a function of rice variety (Rc82, IR64, Rc18) and transplanting date (early, middle, late January and July).

hydrology, temperature, rainfall pattern, and the availability of irrigation, farmers do not plant their crops on the same date, resulting in inter-field variations. These variations in planting date are reflected in variations in radar backscatter among fields within a region. To identify rice fields, Le Toan *et al.* (1997) found that the standard classification methods, which are based on the similarity in the image intensity, are not appropriate. They proposed and tested a temporal change measurement method to cope with inter-field variation due to differences in crop calendar, using ERS-2 SAR. Liew *et al.* (1998) used a similar approach to create five threshold change index maps from six ERS-2 SAR images to delineate area under rice production.

Neural network classification provides consistent and reliable results, given the availability of appropriate ground data to train the network. However, within the context of an operational rice mapping system, variations in the rice crop calendar across a region would make it extremely difficult to acquire sufficient ground data to characterize all rice fields. For example, in the regions centred on Muñoz and Santo Domingo, the rice calendar during some wet seasons can span up to 70 days, as some farmers plant their rice fields in early June, while others delay planting until the middle of August. In this particular study, the ground data collected during the vegetation phase covered a period of only 30 days. In order to map the rice production area on a regional basis, given that the timing of the rice crop calendar varies across a region, this project proposes a method that integrates a change detection approach with a neural network classification. The results of four methods for rice acreage mapping – change detection, neural network classification, maximum likelihood classification, and an integrated change detection neural network approach – are compared.

4.1 *A change detection method for rice mapping*

The change detection method was based on simple ratioing of two RADARSAT-1 images. Using this approach, rice fields were identified as a function of the degree of change in backscatter ($\Delta\sigma^\circ$) between two images. A threshold value was identified and pixels with a change value above this threshold were retained within the rice class. The algorithm used in the ratioing process is as follows (Rignot and van Zyl 1993):

$$\Delta\sigma^\circ = 20 * \log\left(\mathrm{P_j}/\mathrm{P_i}\right) \tag{1}$$

where $\mathrm{P_i}$ and $\mathrm{P_j}$ represent the radar backscatter in amplitude from two consecutive images, i and j. The output of the ratioing process was a difference image, expressed in decibels. Positive values indicated that for the jth image, backscatter was higher relative to the ith image. Negative values meant the reverse was true, and zero (or close to zero) values meant that there was little or no difference in backscatter between the two images.

In determining the threshold value, both SAR speckle and image registration errors must be taken into consideration. The probability that a detected change is false is related to the value of the threshold. A larger threshold tends to underestimate the rice area, whereas a smaller threshold increases the probability of false detection. For the data in this study, a threshold of $\pm$ 3 dB provided the best compromise between over and under estimation. A 3 dB threshold was also used by Ribbes and Le Toan (1999).

Since farmers do not plant their rice crop at the same time, one of the advantages of the change detection approach is that this method permits the delineation of rice fields cultivated at different times during a rice production season. By retrieving information on cultivation date, knowledge is gained about farmers' practices in the region; information that is also needed for rice yield prediction.

4.2 *A neural network method for rice mapping*

Neural networks are computational models with the ability to 'learn' or to organize data based on a parallel processing system (Erbek *et al.* 2004). In order for a neural network to perform a task, such as image classification and modelling, a network has to go through a learning process to memorize the pattern and to learn the relationship between cause and effect (Pao 1989). The performance of a neural network depends on both the network structure as well as the learning parameters. The number of layers and the number of neurons in each layer define the network structure. The learning parameters include learning rate, momentum, and convergence threshold (iterations). Learning rate and momentum play similar roles in neural network learning. The larger the momentum and learning rate, the bigger the step required to minimize the system error. However, a higher learning rate affects the stability of the network training, thus a smaller learning rate and a larger momentum were used in this experiment.

The choice of design of the network architecture and the values of the learning rate parameters is not straightforward. There are no given rules for configuration of the network. Usually, the best results are obtained by trial and error, although it is impractical to try and test all combinations. In this study, a hierarchical procedure was used to find the best network structure and combination of learning parameters. Different neural networks were evaluated, in terms of the accuracy of rice field mapping, in a smaller test area with 512×512 pixels. There were 24 rice fields, 6 fishponds, and 16 non-rice fields selected within this test area. The ground data were processed on a field basis and were divided into a training (21) and test (25) set. Six radar images from 1st January to 23rd February (table 1) were used in this analysis, as the network input. No speckle filtering was applied. Different network structures and training cycles (iterations) were first tested, with all other parameters held constant. Once the structure and iterations were determined, only the learning rate and momentum were varied. This exercise used the same training and test datasets as those used to determine the network structure and number of iterations. Testing results were evaluated in terms of the average mapping accuracy of each class.

Figure 3 presents the mapping accuracies for the test site, as a function of the neural network structure and learning cycle. The legend indicates the number of

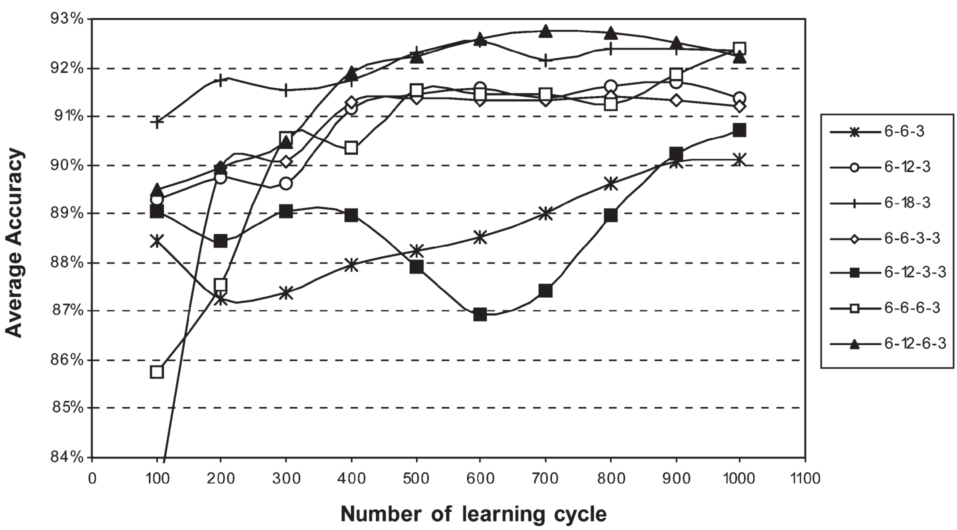

Figure 3. Rice mapping accuracies for various neural network structures and learning cycles.

neurons in each layer. A sequence of three numbers indicates a network with one hidden layer and a sequence of four numbers represents a two hidden layer network. For each sequence, the first and last numbers represent the number of neurons in the input and output layers, respectively. The six input layers represent the six RADARSAT-1 images. The three output layers include rice, non-rice, and fishponds. The middle values give the number of neurons in each hidden layer. For instance, 6-12-3 indicates that this is a one hidden layer neural network with 6, 12, and 3 neurons in the input, hidden, and output layers. In contrast, 6-12-6-3 is a two hidden layer network with 12 and 6 neurons in each hidden layer.

With the exception of the structure 6-12-3-3, the mapping accuracy increased as the learning cycle increased, reaching the highest accuracies at around 400 to 700 iterations. As the learning cycle continued to increase from 700 to 1000 iterations, the mapping accuracy tended to be stable. There were two neural networks, 6-18-3 and 6-12-6-3, which out-performed the other networks. The selection of network 6-12-6-3 was preferred as it produced the highest accuracy. The trend observed for the 6-12-6-3 network is desirable, since this structure will likely produce stable mapping results in a relatively larger dynamic range of training time and will be easily optimized. The network structure of 6-12-3-3 performed poorly. The difference between the 6-12-6-3 and 6-12-3-3 structures is only the number of neurons in the second hidden layer. This observation is consistent with the results obtained by Chen (1997) for wheat crop monitoring. Chen (1997) reported that for a two-layer neural network, the best results were obtained when the number of neurons in the first hidden layer is greater than the input features and when the number of neurons in the second hidden layer is neither close to that of the first hidden layer nor close to that of the output layer.

4.3 *Comparing mapping accuracies using a change detection, a neural network, and an integrated approach*

The accuracies of several classification methodologies for identifying rice fields were assessed against ground data collected during the dry season. Results were compared between the change detection and neural network approaches. In addition, a new integrated approach is introduced and accuracy results are presented. The mapping accuracies of these three methods were also compared to results from a maximum likelihood classification (MLC).

The classifications were run for the same test site described in the previous section. Due to the availability of ground data in this smaller test site, only the first six images in the dry season (1st January to 23rd February in table 1) were used in this comparison. A colour composite of three of the RADARSAT-1 images (1st January, 18th January, and 18th February) is provided in figure 4(*a*). In figure 4(*b*), the samples of the ground data were superimposed on the composite image. Differences in the planting dates were reflected in differences in the radar backscatter observed among the rice fields in the area. Rice fields with a bluish tone were planted in early January; fields with a red to orange tone were planted in mid to late February.

To train the neural network and the MLC, the ground data acquired in this area were evenly divided into training and test sets. The test dataset was used to evaluate the mapping accuracies for all four methods. For all methods, the results were compared using input images with and without speckle filtering applied. Both 3×3 and 5×5 gamma filters were evaluated. Three classes or outputs were

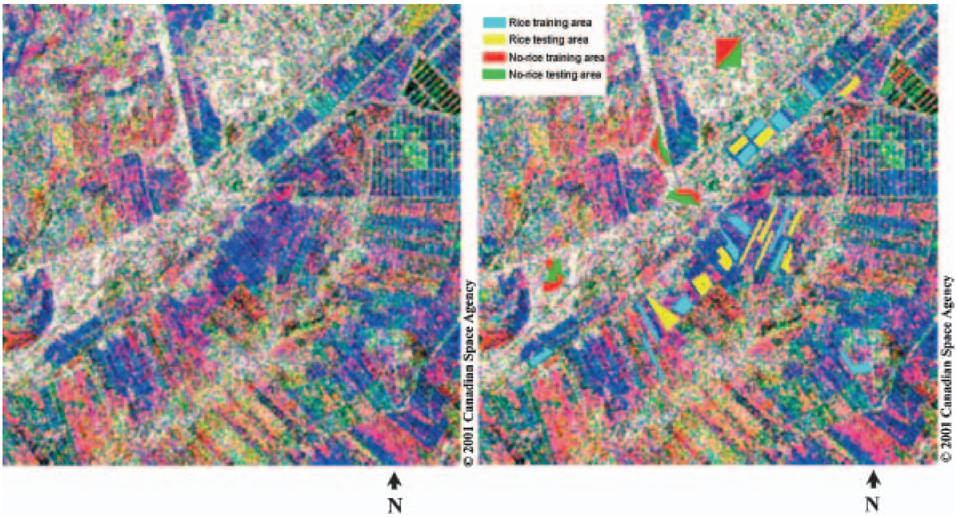

(*a*) (*b*)

Figure 4. Colour composite of RADARSAT-1 images. (*a*) 1st January displayed as red, 18th January as green and 18th February as blue. (*b*) Composite image with a sample of the training and testing sites overlaid.

requested – rice, water features, and no-rice. The water features and no-rice were then merged into a single no-rice class. A sieve filter, which merges smaller polygons with neighbouring classes, was applied to all the mapping results. The size of the merged polygon was set to 0.0075 hectares (3 pixels of RADARSAT-1 fine mode imagery).

For the change detection approach, five ratio images were created from the six individual RADARSAT-1 images. The ratio images included: (1) 6th January/1st January; (2) 18th January/6th January; (3) 30th January/18th January; (4) 11th February/30th January; and (5) 23rd February/11th February. For each ratio image, rice fields were identified using the $\pm$ 3 dB threshold. Finally, fields identified as rice on each ratio image were merged into a single rice map. The results of the change detection approach, with and without speckle filtering, are given in figure 5(*a–c*).

The classified images generated by a maximum likelihood classification (MLC) are shown in figure 5(*d–f*). The neural network maintained the two hidden layer structure (6-12-6-3) using the six RADARSAT-1 images as the inputs and requesting the three output classes. The neural network maps are given in figure 5(*g–i*). The networking training parameters were: momentum 0.9, learning rate 0.1, and learning cycle 700.

Assessments of these three classification methodologies are listed in table 2 in terms of the mapping accuracy and the Kappa coefficient. The average accuracy is defined as average of the accuracies for each class, and the overall accuracy is a similar average with the accuracy of each class weighted by the proportion of test samples for that class. The Kappa coefficient accounts for errors of omission and commission and the effects of chance agreement (Lillesand and Kiefer 2000). The Kappa coefficient is thus considered a more robust indicator of classification accuracy. With no speckle filtering applied, both the MLC and the neural network achieved overall mapping accuracies of 91% and 92%, respectively. The change detection performed poorly without a speckle filter, although the overall classification accuracy improved once a filter was applied. However, application

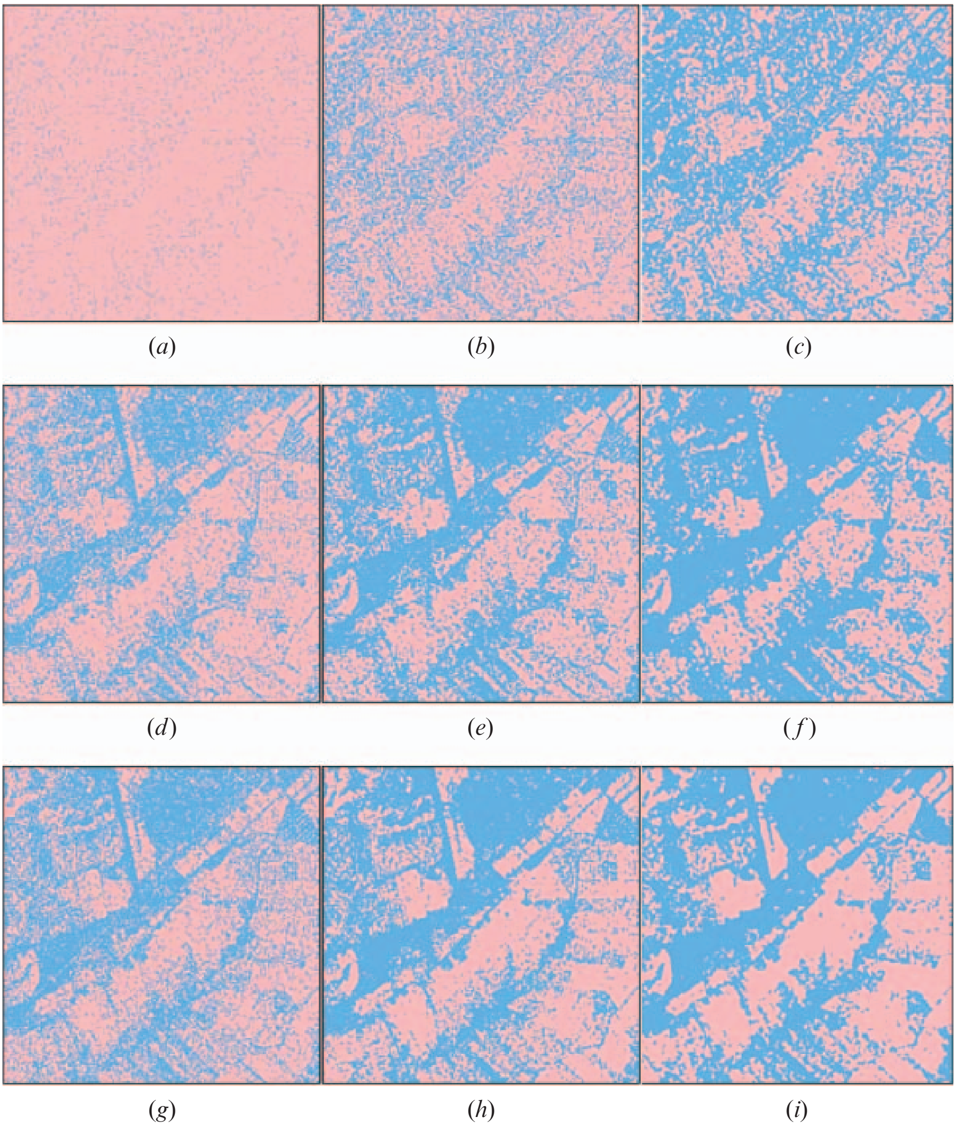

Figure 5. Rice mapping results. Pink represents rice and blue non-rice. (*a*) Change detection without filter; (*b*) change detection with 3×3 gamma filter; (*c*) change detection with 5×5 gamma filter; (*d*) MLC without filter; (*e*) MLC with 3×3 gamma filter; (*f*) MLC with 5×5 gamma filter; (*g*) neural network without filter; (*h*) neural network with 3×3 gamma filter; (*i*) neural network with 5×5 gamma filter.

of a filter reduced the accuracy with which the change detection method identified rice fields. A similar trend was observed in the MLC results. Application of a speckle filter increased the accuracy of mapping non-rice fields, but decreased the accuracy with which rice fields were identified. The neural network was superior to either method, especially when a larger filter was applied. Without a filter, the classified map produced by the neural network had an overall accuracy of 92%. When the six input images were filtered using a 5×5 gamma filter, an overall accuracy of 99% was achieved with the neural network approach.

Table 2. Accuracy assessment for change detection, MLC, and neural network classification methodologies.

Change detection						
	no filtering		**3 × 3 gamma filter**		**5 × 5 gamma filter**	
	rice	**non-rice**	**rice**	**non-rice**	**rice**	**non-rice**
Rice	96.6	3.4	86.0	14.0	77.6	22.4
Non-rice	90.8	9.2	53.2	46.8	22.1	77.9
Average accuracy	0.53		0.66		0.78	
Overall accuracy	0.69		0.73		0.78	
Kappa coefficient	0.07		0.35		0.52	
Maximum likelihood classification						
	no filtering		**3 × 3 gamma filter**		**5 × 5 gamma filter**	
	rice	**non-rice**	**rice**	**non-rice**	**rice**	**non-rice**
Rice	92.8	7.2	85.8	14.2	81.2	18.8
Non-rice	13.4	86.6	3.2	96.8	0.1	99.9
Average accuracy	0.90		0.91		0.91	
Overall accuracy	0.91		0.89		0.87	
Kappa coefficient	0.79		0.77		0.73	
Neural network mapping						
	no filtering		**3 × 3 gamma filter**		**5 × 5 gamma filter**	
	rice	**non-rice**	**rice**	**non-rice**	**rice**	**non-rice**
Rice	90.9	9.1	97.4	2.6	99.2	0.8
Non-rice	6.1	93.9	0.4	99.6	0.0	100.0
Average accuracy	0.92		0.99		1.00	
Overall accuracy	0.92		0.98		0.99	
Kappa coefficient	0.82		0.96		0.99	
Integration of change detection and neural network						
	no filtering		**3 × 3 gamma filter**		**5 × 5 gamma filter**	
	rice	**non-rice**	**rice**	**non-rice**	**rice**	**non-rice**
Rice	87.4	12.6	95.5	4.5	98.9	1.1
Non-rice	3.1	96.9	0.4	99.6	0.1	99.9
Average accuracy	0.92		0.98		0.99	
Overall accuracy	0.90		0.97		0.99	
Kappa coefficient	0.79		0.93		0.98	

The neural network classification out-performed both the change detection and the maximum likelihood classification approaches. However, neural networks require extensive and representative training data. Even within a relatively small site, such as the one used here, the available ground data can be limited. But considering much broader regions, where planting dates can vary substantially, it is often not possible to collect enough representative training data. In order to map the rice production area on a regional basis and to cope with the variations in the rice calendar, a method was developed which integrates both the change detection and the neural network approaches. In this integrated method, the neural network training data were extracted from the change detection results. With this approach, the neural network was able to map rice fields over a much larger area, setting the stage for operational implementation. The generalized processing steps of this integrate approach are as follows:

1. create a change detection map from the RADARSAT-1 imagery;
2. generate random samples for rice and non-rice from the change detection map;
3. on-screen editing to exclude outliers;
4. neural network training and classification using inputs of RADARSAT-1 imagery; and
5. perform accuracy assessment.

The results from this integrated approach were compared to those generated by the other three methods, using the same test data. Figure 5(*c*) was used as the change detection map. From this map, 2% of the samples were randomly selected. These pixels were then edited on-screen, using the image as shown in figure 4(*a*). This allowed pixels that fell outside of the rice fields to be excluded. The edited rice pixels, along with the pixels identified as non-rice, were used to train a neural network with the same structure and parameters as previously chosen. Figure 6(*a–b*) show the results from this integrated method, where 6(*a*) is the result with no speckle reduction applied to the RADARSAT-1 images prior to the neural network classification. In figures 6(*b*) and 6(*c*), a 3×3 and a 5×5 gamma filter have been applied prior to the mapping process. The accuracy assessment of the integrated method is provided in table 2. The overall mapping accuracy of figures 6(*a*), 6(*b*), and 6(*c*) was 90%, 97%, and 99%, respectively.

4.4 *Rice mapping at a larger regional scale using the integrated change detection neural network approach*

A classification method which integrates a change detection and a neural network approach provides a high level of accuracy, without the requirement for significant ground data to train the network. To test the application of this integrated approach at a larger regional scale, this method was applied to the entire area incorporating both Muñoz and Santo Domingo. This integrated classification was run for both the dry and wet seasons, thus testing the robustness of this approach under different rice

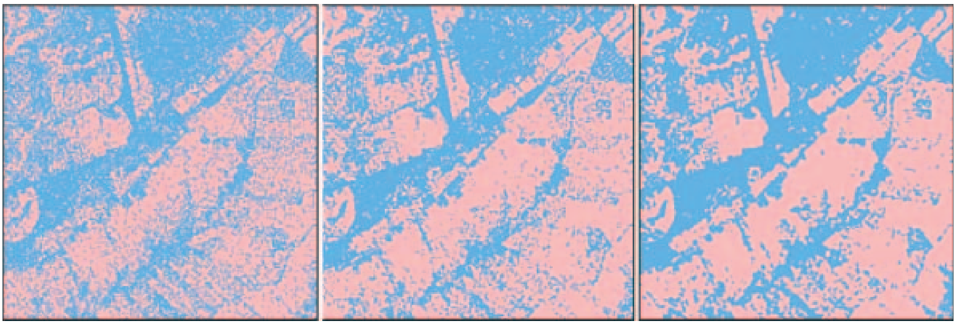

(*a*) (*b*) (*c*)

Figure 6. Rice mapping results from the integrated change detection and neural network method. Pink represents rice and blue non-rice: (*a*) without a filter; (*b*) with a 3×3 gamma filter; and (*c*) with a 5×5 gamma filter.

growing conditions. The wet season runs from early June to early October. A colour composite image of 5th July, 29th July, and 22nd August is displayed as red, green, and blue in figure 7(*a*). According to the developed methodology, change occurrence images were first created from the RADARSAT-1 images. These change images were then combined to create a series of rice maps representing various planting periods throughout the growing season. A final integration of these maps resulted in a single rice map with a series of rice classes based on planting period.

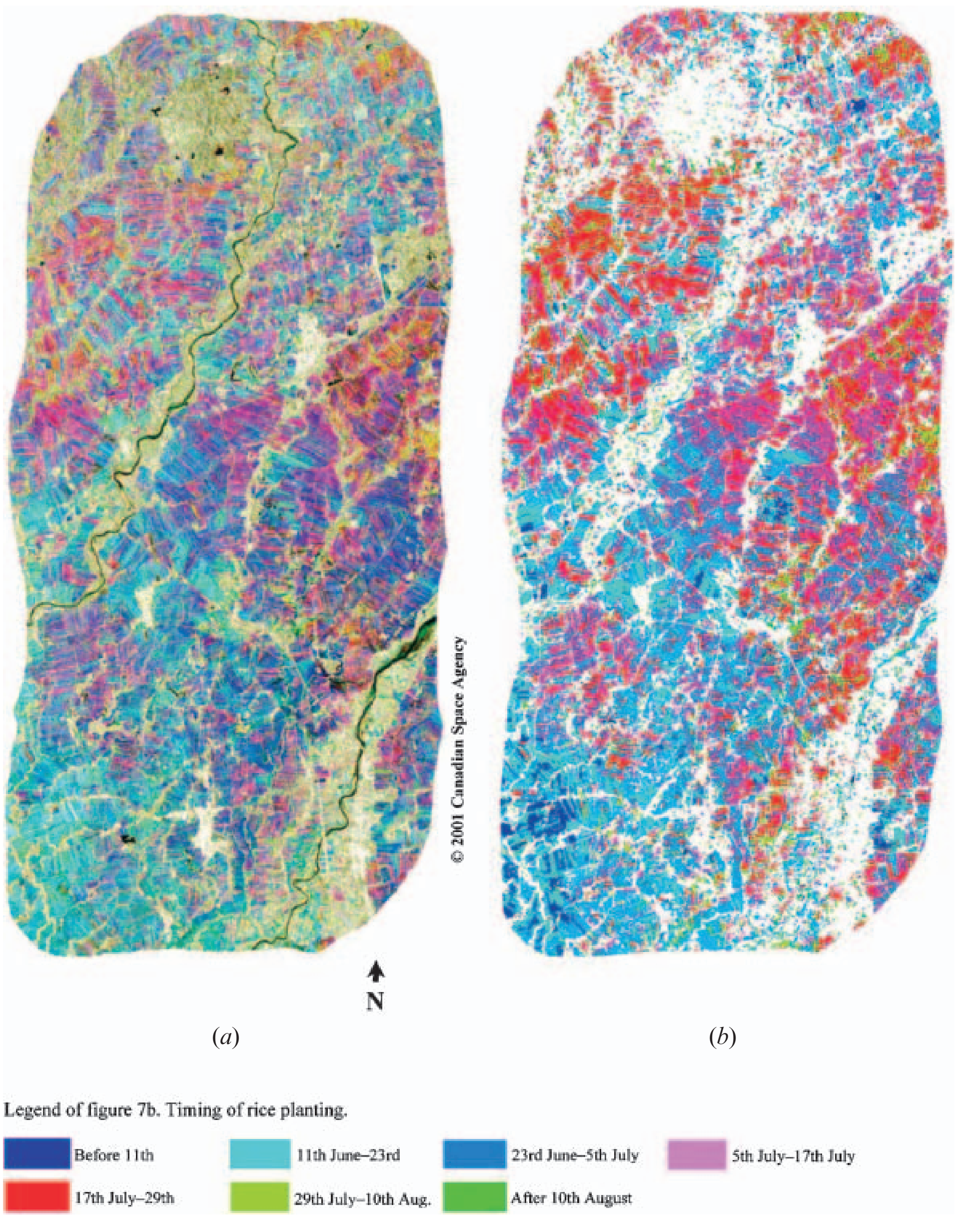

Figure 7. Rice map from change detection approach. (*a*) Colour composite of RADARSAT-1 images with 5th July displayed as red, 29th July as green and 22nd August as blue. (*b*) Detected rice fields. The colour codes indicate the planting periods of the rice fields.

A 5×5 gamma filter was applied to all RADARSAT-1 imagery. The change occurrence images were created from these filtered images using the ratio of the first and last image acquisitions, as well as image pairs acquired 24 days apart. A 3 dB threshold was applied to identify rice fields. Two sets of change images were created. The first set of ratio images are from the RADARSAT-1 fine mode 3 (ascending) acquisitions; the second set from the fine mode 1 (descending) passes. The ratio images created for the wet season are given below:

Set 1: 1/9; 3/1; 5/3; 7/5
Set 2: 2/10; 4/2; 6/4; 8/6

where 1 to 10 represents the images acquired on 11th June, 23rd June, 5th July, etc., according to the list of acquisitions given in table 1. The ratios were calculated according to equation (1).

Variations in planting dates across this large region meant that no single image pair or change occurrence image could identify all rice fields. Therefore, rice maps created from the same RADARSAT-1 orbit were combined. A further integration of rice maps between the two orbits (set 1 and set 2) resulted in a single classified image, with seven rice classes corresponding to seven planting periods.
Set 1:

1/9 **AND** 3/1 $\rightarrow$A transplanted before 11th June
3/1 **AND** 5/3 $\rightarrow$B transplanted between 11th June and 5th July
5/3 **AND** 7/5 $\rightarrow$C transplanted between 5th July and 29th July
7/5 $\rightarrow$D transplanted between 29th July and 22nd August

Set 2:

2/10 **AND** 4/2 $\rightarrow$ A′ transplanted before 23rd June
4/2 **AND** 6/4 $\rightarrow$ B′ transplanted between 23rd June and 17th July
6/4 **AND** 8/6 $\rightarrow$ C′ transplanted between 17th July and 10th August

where **AND** indicates a logical AND operation.

The seven planting periods (t1 to t7), in 12-day intervals, were extracted according to the following logic.

A **AND** A′ $\rightarrow$ transplanted before 11th June ....(t1)
A′ **AND** B $\rightarrow$ transplanted 11th June–23rd June ....(t2)
B **AND** B′ $\rightarrow$ transplanted 23rd June–5th July ....(t3)
B′ **AND** C $\rightarrow$ transplanted 5th July–17th July ....(t4)
C **AND** C′ $\rightarrow$ transplanted 17th July–29th July ....(t5)
C′ **AND** D $\rightarrow$ transplanted 29th July–10th August ....(t6)
D $\rightarrow$ transplanted after 10th August ....(t7)

For the wet season, the rice map generated by this change detection approach is presented in figure 7(*b*). Seven rice classes, corresponding to the rice transplanting periods, are represented on the map. For reference, a three-colour composite is provided in figure 7(*a*). In the south-west region, bluish tones indicate that the farmers planted their rice earlier in the wet season, while the farmers in the north-east region delayed their planting by about two months. According to the rice map, the rice calendar gradually shifts from south-west to north-east. The majority of farmers however, planted their fields in July, in the middle of the planting season.

To train the neural network, two per cent of the pixels from these rice maps were randomly selected and the outliers were excluded through on-screen editing. All RADARSAT-1 images were used as input. The input of the network consisted of 10, the output of 7, and the two hidden layers were 20 and 14, respectively. According to the results from the test site, a 5×5 gamma filter provided the highest mapping accuracy. However, considering the rice fields across the region are small and narrow, a 3×3 gamma filter was used in this application to suppress the radar speckle. A neural network with two hidden layers was used with 20 and 14 neurons for the first and second hidden layers, respectively. Momentum was set to 0.9, learning rate to 0.1, and learning cycle to 700. Figures 8 and 9 present the results of the neural network classification for Muñoz and Santo Domingo. These maps (figures 8(*b*) and 9(*b*)) identify the rice-cultivated land for the 2001 wet season. The classes associated with the timing of rice planting are presented in figures 8(*c*) and 9(*c*).

For both seasons, the accuracy of rice field mapping using this integrated approach was assessed on both a field and a regional basis. At the local level, the classification accuracy of all 56 fields surveyed during the ground collection campaign was assessed. At the regional level, rice acreage statistics were derived from the classification and were compared with the statistics from the Department of Agriculture of Nueva Ecija in the Philippines. These government statistics are obtained through quarterly nationwide surveys. The sampling strategy for the surveys involves a two-stage stratified sampling, with the barangay (a unit of local administration) as the primary sampling unit and the farm household as the secondary or ultimate sampling unit. The survey generates information on the palay (unmilled rice) area, production, yield, feed and fertilizer uses, among other things (PhilRice 2000).

At the local level, the overall classification accuracy for the rice fields visited during the field campaign was 97%, for the wet season. For the dry season, the accuracy was slightly lower at 96%. Table 3 compares the statistics derived from the integrated mapping approach to the government statistics reported for both Muñoz and Santo Domingo. The ratio of rice acreage to total acreage, for both the government and classification estimates, is compared in this table. For the dry season, the integrated approach produced very comparable results, to within 3% of the government reported data. However, for the wet season, the integrated approach overestimated the rice acreage (relative to the total acreage) by about 6% for the Santo Domingo region. At both the local and regional scales, this integrated approach was able to identify rice fields and also provided an accurate assessment of rice acreage.

5. Predicting rice yield using a neural network

Rice classification maps are required for yield prediction. Two yield prediction neural networks were developed using yield data acquired during the 2001 wet season. Two sets of yield data were acquired; one set of yield data was acquired during the field experiment by collecting sample data from the rice plots. The second set of yield data are estimates given by farmers during interviews with government officials. For some rice fields, the difference between these two yield estimates was drastic. For example, the experimental yield data collected for field 2C2 was 5514 kg, while the farmer's yield estimate for the same field was 7997 kg, a difference of more than two thousand kilograms. The yield data measured for field 2A9 was

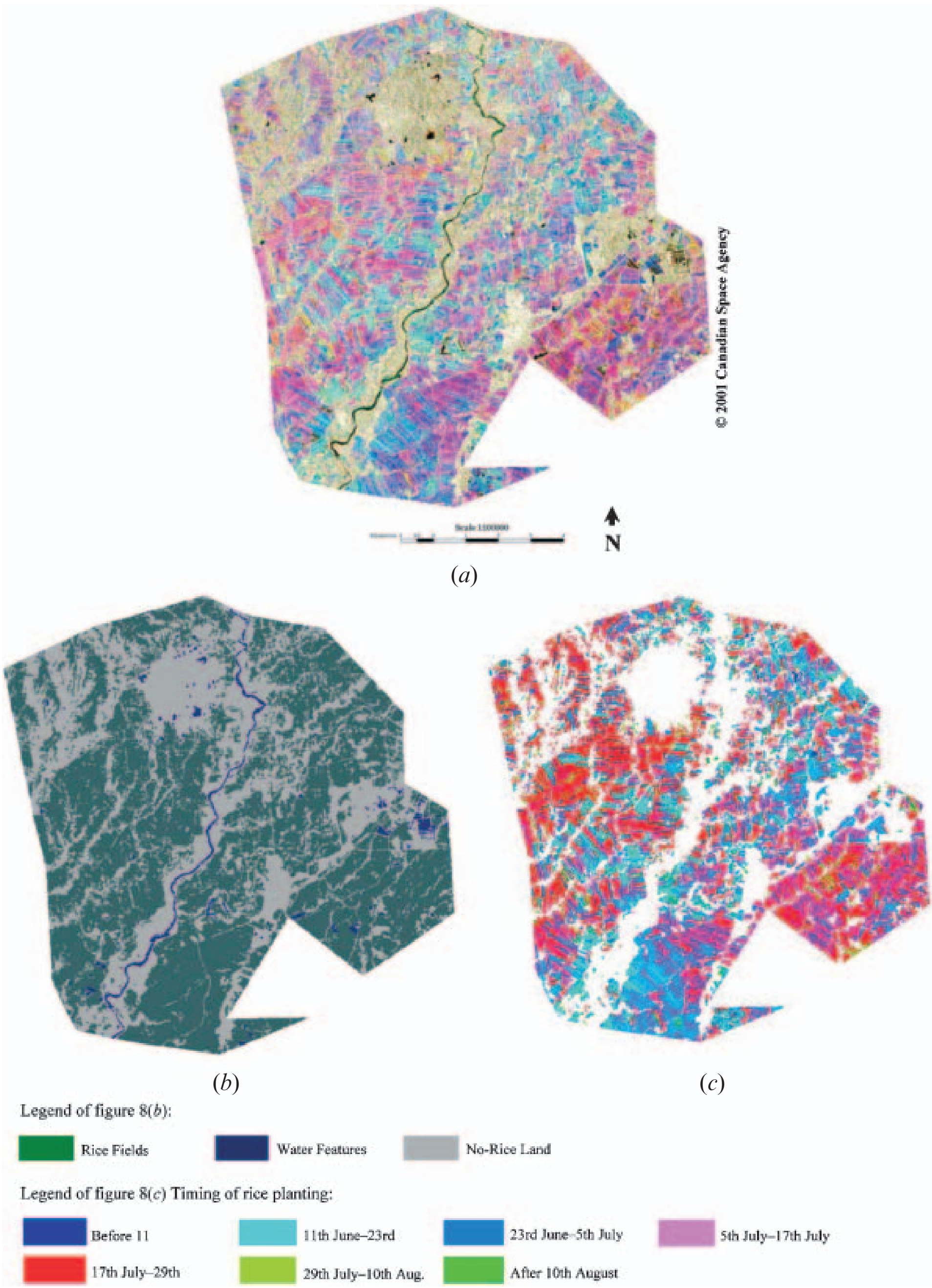

Figure 8. Integrated neural network classification results of Muñoz for the 2001 wet season. (*a*) A colour composite of 5th July displayed as red, 29 July as green and 22 August as blue; (*b*) results from the first level classification with three classes: rice-growth area, no-rice land, and water; (*c*) rice fields colour coded according to the period of planting.

10,197 kg, compared to an estimated 6250 kg, the field measurements nearly double that of the farmer's estimate. Experience during the 2001 dry season led to an improvement in the yield data collection strategy during the following wet season

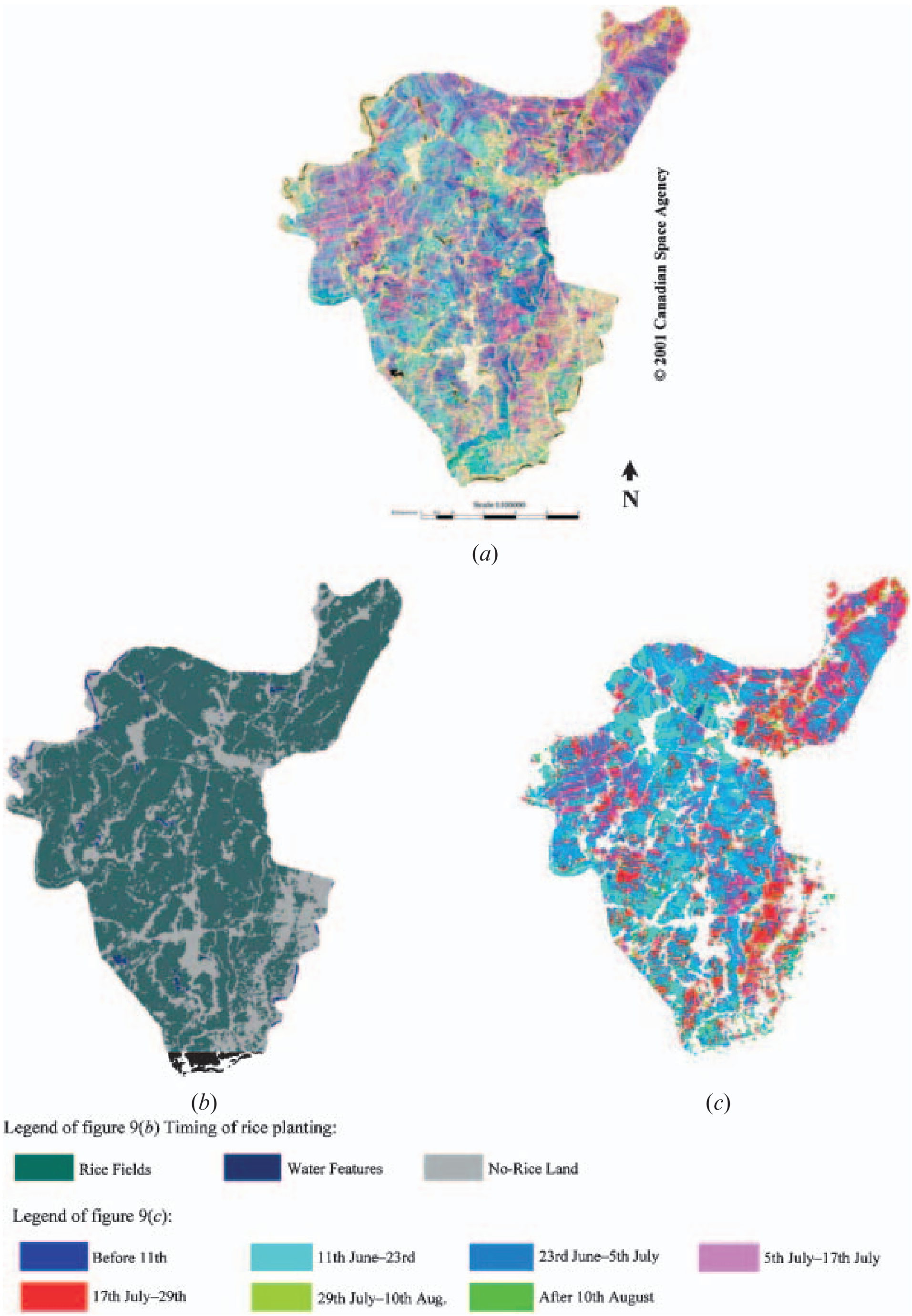

Figure 9. Integrated neural network classification results of Santo Domingo for the 2001 wet season. (*a*) A colour composite of 5th July displayed as red, 29th July as green and 22nd August as blue; (*b*) results from the first level classification with three classes: rice-growth area, no-rice land, and water; (*c*) rice fields colour coded according to the period of planting.

Table 3. Accuracy of rice field mapping using integrated approach compared to government reported statistics.

Dry season, 2001	**Statistics from Dept. of Agriculture**		**Experimental results (Estimated Acreage)**		**% Rice field mapped** $\left(\frac{A/B}{C/D}\right)$
	A	B	C	D	
	Total land (ha)	Rice area harvested (ha)	Total land mapped (ha)	Rice area mapped (ha)	
			Muñoz		
Integrated approach	16,305	5,250.74	16,005.78	5,307.23	102.97%
			Santo Domingo		
Integrated approach	9,569	6,177.07	9,258.95	5,840.45	97.72%
Wet season, 2001	**Statistics from Dept. of Agriculture**		**Experimental results (Estimated Acreage)**		**% Rice field mapped** $\left(\frac{A/B}{C/D}\right)$
	A	B	C	D	
	Total land (ha)	Rice area harvested (ha)	Total land mapped (ha)	Rice area mapped (ha)	
			Muñoz		
Integrated approach	16,305	9,358.39	16,005.78	9,343.52	101.71%
			Santo Domingo		
Integrated approach	9,569	6,467.91	9,258.95	6,650.81	106.27%

field campaign. Although the methodology was improved for the wet season data collection by increasing the number of samples gathered within the plots, large inconsistencies between the two yield estimates were still observed. Without further evidence, it is difficult to independently determine the accuracy of either yield dataset. However, by comparing the yield data collected from the rice plots with radar backscatter, it was possible to identify and remove fields that, for this experimental dataset, can be considered as outliers. These fields were identified through an iterative multiregression analysis using the radar backscatter from all RADARSAT-1 images and the yield data collected from the rice plots. Using the backscatter associated with the seven planting periods (t1 to t7), there were seven independent variables used in the multiregression analysis. After the first iteration, samples with regression residuals greater than 1500 were removed. The threshold of residuals was then set to 1000 and then to 600. After the second and third iterations, 47 and 30 field plots were retained and subsequently used to train the neural networks. The networks trained with 30 plots and 47 plots were labelled as Net1 and Net2, respectively. Both Net1 and Net2 used a two-layer neural network with a 6-12-2-1 structure. The inputs were backscatter values associated with the six RADARSAT-1 images used in the neural network approach to rice mapping. The output was the predicted yield for each plot. The training parameters were: momentum 0.9 and learning rate 0.7. The network iteration was determined by varying the number of iterations between 500 and 100,000. An iteration of 60,000 was finally selected as it provided the best training result and prediction dynamics. The classes of rice cultivation (t1 to t7) derived from the integrated change detection approach were used to generate a mask of rice fields and the yield was then predicted for the region under the mask.

The prediction results were assessed using both ground data and the statistics collected by the Philippine government, as previously described. To conduct the comparison with the ground data, the mean yield for each field was extracted from the yield prediction map produced from the neural network. It should be noted that the predicted mean yield for a field could be quite different from the yield used during the network training process for the same field. This is because the predicted mean yield for a field is the average of the predicted yield of each pixel in that field. The yield data used in the training process were the average of four ground samples per plot. The discrepancies between the yield measured on the ground and the neural network prediction are given in figures 10(*a*) (Net1) and 10(*b*) (Net2) for all of the rice plots. The discrepancies between measured and predicted yield are depicted as bars on these figures. Since the data were not sorted by the field numbers (rather by the yields for unfolding the prediction dynamics), and due to the limitation of the graphic size, not all the fields were explicitly displayed in figure 10.

The output yield data from the yield prediction model were grouped by 1000s for the purpose of display and calculation of statistics. For the surveyed fields, when the field average yield predicted by the model was compared to the yield data collected during the ground campaign, 49% of the fields were predicted with an error under 500 kg/ha using Net1 (figure 10). Using Net2, 37% of fields had prediction errors under 500 kg/ha. With an error threshold of 1000 kg/ha, the prediction accuracy increased to 76% and 69%. Only 8% (Net1) and 12% (Net2) of fields had prediction errors greater than 2000 kg/ha. The neural network trained with 30 plots performed better than that trained with 47 plots. However, the yield predicted using Net1 had a lower dynamic range relative to Net2, since more outliers were eliminated.

Rice yield was also predicted for the entire Muñoz and Santo Domingo regions. The predicted yield maps for the wet season for Muñoz and Santo Domingo are presented in figure 11(*a–d*). Figures 11(*a*) and 11(*b*) show the yield prediction results from Net1 and figures 11(*c*) and 11(*d*) are the results from Net2.

For both regions, the rice yield predicted from Net1 and Net2, and the yield reported by the Department of Agriculture in the Philippines, are presented in table 4.

The yield predicted from the neural network is categorized in ranges of thousands. In each category, the mean yield was used in the calculation. The rice cultivated land, predicted yield, and the distribution of the yield from each category were calculated and are listed in the table. The totals from the neural network prediction and from the government statistics are displayed in bold.

The distribution of predicted yield from Net1 for both Muñoz and Santo Domingo was around 3000–6000 kg/ha, with more than 50% of the total yields in the range of 4000–5000 kg/ha. This distribution is comparable to the distribution reported in the government statistics. The average yields from the government statistics were 4420 kg/ha (Muñoz) and 4550 kg/ha (Santo Domingo). The distribution of predicted yield from Net2 was much broader, with 49% of the fields in the 5000–6000 kg/ha category. Comparing predicted average yield to the government statistics, the predicted yield from Net1 is about 6% higher. Net2 yield predictions were about 3% lower than government statistics. Thus, if average yields over the region are considered, the neural network achieved a minimum 94% prediction accuracy. The neural network performed well at predicting total tons of rice and average yields (tons/ha) on a regional basis.

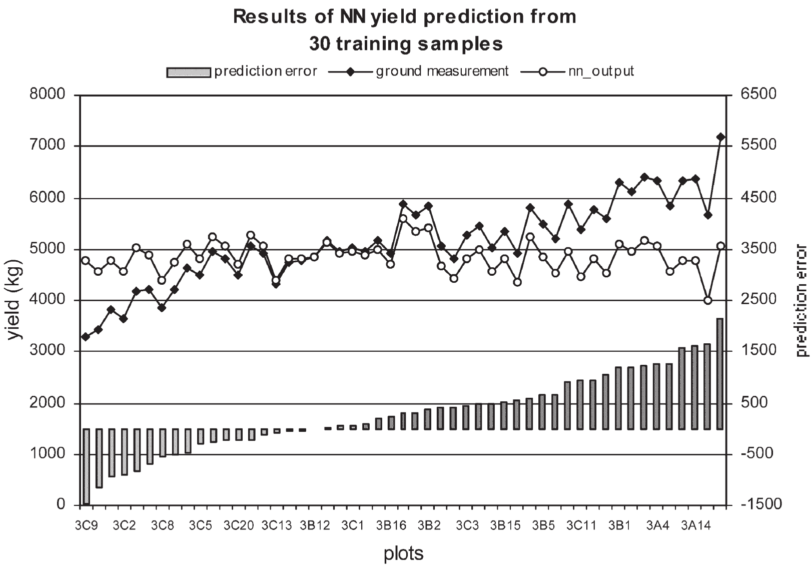

(*a*)

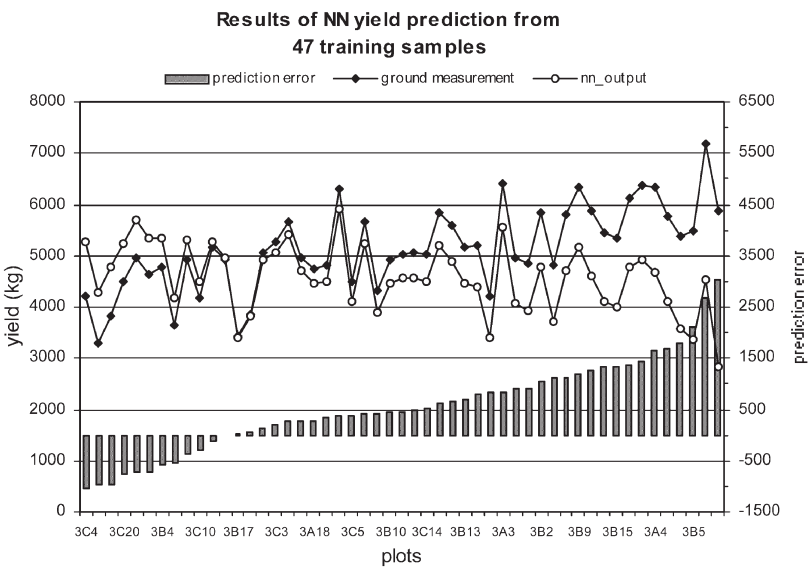

(*b*)

Figure 10. Yield prediction results for all rice plots. (*a*) Neural network trained with 30 samples; (*b*) neural network trained with 47 samples.

6. Conclusions

The primary objective of this project was to develop a methodology to use RADARSAT-1 imagery to effectively map rice production areas, to monitor rice growth, and to predict rice yields. A substantial goal was to develop a rice

Figure 11. Yield prediction results for Muñoz and Santo Domingo. (*a*) and (*b*) results from Net1, where the neural network was trained with 30 plots; (*c*) and (*d*) results from Net2, where the neural network was trained with 47 plots.

monitoring system that would be capable of running operationally. From January 2001 to November 2001, two field campaigns were conducted in the northern part of the province of Nueva Ecija in the Philippines, where the centre of the Philippine Rice Research Institute (PhilRice) is located. To meet the project objectives, a change detection approach was integrated with a neural network. This method was then used to delineate rice production areas and also to extract information on rice

Table 4. Predicted yield compared to statistics from the Department of Agriculture.

	Muñoz					
Wet season, 2001	**30 training plots used (Net1)**			**47 training plots used (Net2)**		
Yield range (kg)	Predicted rice fields (ha)	Predicted yield (tons)	Distribution of yield (%)	Predicted rice fields (ha)	Predicted yield (tons)	Distribution of yield (%)
1,000–2,000				966.75	1,563.58	3.85
2,000–3,000	1.49	4.31	0.010	1,200.89	3,009.33	7.41
3,000–4,000	1,041.21	3,910.43	8.830	1,312.96	4,610.47	11.35
4,000–5,000	5,035.11	22,907.89	51.730	1,654.12	7,495.93	18.46
5,000–6,000	3,171.01	16,877.42	38.112	3,623.28	19,997.61	49.25
6,000–7,000	94.68	583.79	1.318	422.02	2,748.71	6.77
7,000–8,000	0.01	0.07	0.000	163.50	1,182.22	2.91
			Average yield (tons)/ha^{-1}			***Average yield (tons)/ha^{-1}***
Totals from prediction	***9,343.51***	***44,283.9***	***4.75***	***9,343.52***	***40,607.85***	***4.32***
Totals from statistics	***9,358.39***	***41,330.96***	***4.42***	***9,358.39***	***41,330.96***	***4.42***

	Santo Domingo					
Wet season, 2001	**30 training samples used**			**47 training samples used**		
Yield range (kg)	Predicted rice fields (ha)	Predicted yield (tons)	%	Predicted rice fields (ha)	Predicted yield (tons)	%
1,000–2,000				565.98	1,101.26	3.77
2,000–3,000	0.64	0.76	0.002	883.98	2,585.33	8.84
3,000–4,000	709.91	2,597.04	8.231	968.07	3,020.56	10.33
4,000–5,000	3,592.68	16,439.05	52.102	1,205.76	4,981.14	17.03
5,000–6,000	2,281.29	12,153.29	38.519	2,573.47	14,372.91	49.14
6,000–7,000	66.29	361.68	1.146	340.83	2,430.40	8.31
7,000–8,000	0.01	0.76	0.002	112.72	755.59	2.58
			Average yield (tons)/ha^{-1}			***Average yield (tons)/ha^{-1}***
Totals from prediction	***6,650.82***	***31,551.82***	***4.76***	***6,650.81***	***29,247.16***	***4.37***
Totals from statistics	***6,467.91***	***29,428.99***	***4.55***	***6,467.91***	***29,428.99***	***4.55***

cultivation as a function of different planting dates. These rice maps were then used in a neural network-based yield model to predict rice yields on a regional basis.

The significant increase in radar backscatter over the short vegetation phase of rice growth alludes to the potential of radar imagery for rice monitoring. The multiple incident angles of RADARSAT-1 provide tremendous flexibility with respect to image acquisition. In this paper, the relationship between rice growth and radar backscatter was examined for both a dry and wet season. RADARSAT-1 imagery was acquired at a twelve-day interval over the study sites. Although rice cultivation practices are different for these two seasons, an 8 dB increase in radar backscatter during the vegetation phase was observed in both seasons. This significant increase in backscatter provided the basis for rice field mapping.

The accuracies of four methods for rice mapping were compared. These methods included a simple maximum likelihood classification, a change detection approach, a neural network classification, and an integrated approach. Rice maps were generated for both the dry and wet seasons. With an integrated change detection and neural network approach, a minimum mapping accuracy of 96% was achieved, for both seasons. Rice yields for the wet season were predicted using a neural network. The result was an encouraging 94% prediction accuracy when the yields predicted by the neural network were compared with government statistics. Results obtained from this study demonstrate the potential of radar imagery for wetland rice crop mapping, monitoring, and yield prediction.

Acknowledgements

We wish to acknowledge the financial support provided by the Canadian Space Agency under the RADARSAT User Development Program. We thank the valuable contributions of the Philippines Rice Research Institute for providing the experimental sites and assistance in field data acquisition, and Ms Joan Pereverzoff for her exceptional organization and management skills in collecting and processing field samples. We wish to specially acknowledge Dr Kit Sarkar, the late president of Devel-Tech Inc., for his vision and dedication to this project.

References

Aschbacher, J., Pongsrihadulchai, A., Karnchanautham, S., Rodprom, C., Paudyal, D.R. and Le Toan, T., 1995, Assessment of ERS-1 data for rice crop mapping and monitoring. In *Proceedings IGARSS*, Florence, Italy, Vol. 3, pp. 2183–2185.

Benediktsson, J.A., Swain, P.H. and Ersoy, O.K., 1990, Neural network approaches versus statistical methods in classification of multisource remote sensing data. *IEEE Transactions on Geoscience and Remote Sensing*, **28**, pp. 540–552.

Bischof, H., Schneider, W. and Pinz, A.J., 1992, Multispectral classification of Landsat images using neural networks. *IEEE Transactions on Geoscience and Remote Sensing*, **30**, pp. 482–490.

Brisco, B. and Brown, R.J., 1995, Multidate SAR/TM synergism for crop classification in western Canada. *Photogrammetric Engineering and Remote Sensing*, **61**, pp. 1009–1014.

Chen, C., 1996, *Artificial Neural Networks in the Application of Remote Sensing – A Primary Study in Artificial Neural Networks.* Report to the National Research Council – Industrial Research Assistance Program (NRC/IRAP), June, 1996, Canada.

Chen, C., 1997, *Crop Biomass Detection by Using Artificial Neural Networks – RADARSAT Application II.* Report to the National Research Council – Industrial Research Assistance Program (NRC/IRAP), August, 1997, Canada.

Erbek, F.S., Ozkan, C. and Taberner, M., 2004, Comparison of maximum likelihood classification method with supervised artificial neural network algorithms for land use activities. *International Journal of Remote Sensing*, **25**, pp. 1733–1748.

Foody, G.M., McCulloch, M.B. and Yates, W.B., 1995, Classification of remote sensed data by an artificial neural network: issues related to training data characteristics. *Photogrammetric Engineering and Remote Sensing*, **61**, pp. 391–401.

Inoue, Y., Kurosu, T., Maeno, H., Uratsuka, S., Kozu, T., Dabrowska-Zeilinska, K. and Qi, J., 2002, Season-long daily measurements of multifrequency (Ka, Ku, X, C, and L) and full-polarization backscatter signatures over paddy rice field and their relationship with biological variables. *Remote Sensing of Environment*, **81**, pp. 194–204.

International Rice Research Institute, 1997, *Rice Almanac, Second edition*.

International Rice Research Institute, 1998, Geography of Production – Regional Overviews, Asia. Available online at: http://www.cgiar.org/irri/riceweb/goverasia.htm (accessed January 25 2002).

KUROSU, T., FUJITA, M. and CHIBA, K., 1995, Monitoring of rice crop growth from space using ERS-1 C band SAR. *IEEE Transactions on Geoscience and Remote Sensing*, **33**, pp. 1092–1096.

LE TOAN, T., RIBBES, F., WANG, L.F., FLOURY, N., DING, K.H., KONG, A., FUJITA, M. and KUROSU, T., 1997, Rice crop mapping and monitoring using ERS-1 data based on experiment and modeling results. *IEEE Transactions on Geoscience and Remote Sensing*, **35**, pp. 41–56.

LI, Y., LIAO, Q., LI, X., LIAO, S., CHI, G. and PENG, S., 2003, Towards an operational system for regional-scale rice yield estimation using a time-series of Radarsat ScanSAR images. *International Journal of Remote Sensing*, **24**, pp. 4207–4220.

LIEW, S.C., KAM, S.P., TUONG, T.P., CHEN, P., MINH, V.Q. and LIM, H., 1998, Application of multitemporal ERS-2 synthetic aperture radar in delineating rice cropping systems in the Mekong River Delta, Vietnam. *IEEE Transactions on Geoscience and Remote Sensing*, **36**, pp. 1412–1420.

LILLESAND, T.M. and KIEFER, R.W., 2000, *Remote Sensing and Image Interpretation, 4th edition* (New York: Wiley).

PARKER, D.B., 1985, *Learning-Logic.* Technical Report TR-47, Massachusetts Institute of Technology, Centre for Computational Research in Economics and Management Science, Cambridge, MA.

PAO, Y.H., 1989, *Adaptive Pattern Recognition and Neural Networks* (Boston, MA: Addison-Wesley).

PAOLA, J.D. and SCHOWENGERDT, R.A., 1995, A detailed comparison of back propagation neural network and maximum-likelihood classifiers for urban land use classification. *IEEE Transactions on Geoscience and Remote Sensing*, **33**, pp. 981–996.

PHILRICE, 2000, *Rice Statistics Handbook, 1970–1997.* A collaborative project of: Department of Agriculture, Philippine Rice Research Institute, Maligaya, Muñoz, 3119 Nueva Ecija and Department of Agriculture, Bureau of Agricultural Statistics, 1184 Ben-Lor Building, Quezon Ave., Quezon City.

RIBBES, F. and LE TOAN, T., 1999, Rice field mapping and monitoring with RADARSAT data. *International Journal of Remote Sensing*, **20**, pp. 745–765.

RIGNOT, E.J.M. and VAN ZYL, J.J., 1993, Change detection techniques for ERS-1 SAR data. *IEEE Transactions on Geoscience and Remote Sensing*, **31**, pp. 896–906.

RUMELHART, D.E., HINTON, G.E. and WILLIAMS, R.J., 1986, Learning representations by back-propagating errors. *Nature*, **323**, pp. 533–536.

SHAO, Y., FAN, X., LIU, H., XIAO, J., ROSS, S., BRISCO, B., BROWN, R. and STAPLES, G., 2001, Rice monitoring and production estimation using multitemporal RADARSAT. *Remote Sensing of Environment*, **76**, pp. 310–325.

WERBOS, P.J., 1974, Beyond regression: New tools for prediction and analysis in the behavioural sciences. PhD thesis, Harvard University, Cambridge, MA.

THE WORLD BANK GROUP, 2000. Available online at: http://www.worldbank.org/depweb/english/modules/glossary.htm#pgr (January 25 2002).